Journal of Nanobiotechnology

RESEARCH Open Access

# Bactericidal effects and accelerated wound healing using $Tb_4O_7$ nanoparticles with intrinsic oxidase-like activity

Chen Li[1†], Yurong Sun[1†], Xiaoping Li[1†], Sanhong Fan[1*], Yimin Liu[2], Xiumei Jiang[3], Mary D. Boudreau[4], Yue Pan[2*], Xin Tian[5*] and Jun-Jie Yin[3]

## Abstract

**Background:** Nanomaterials that exhibit intrinsic enzyme-like characteristics have shown great promise as potential antibacterial agents. However, many of them exhibit inefficient antibacterial activity and biosafety problems that limit their usefulness. The development of new nanomaterials with good biocompatibility and rapid bactericidal effects is therefore highly desirable. Here, we show a new type of terbium oxide nanoparticles ($Tb_4O_7$ NPs) with intrinsic oxidase-like activity for in vitro and in vivo antibacterial application.

**Results:** We find that $Tb_4O_7$ NPs can quickly oxidize a series of organic substrates in the absence of hydrogen peroxide. The oxidase-like capacity of $Tb_4O_7$ NPs allows these NPs to consume antioxidant biomolecules and generate reactive oxygen species to disable bacteria in vitro. Moreover, the in vivo experiments showed that $Tb_4O_7$ NPs are efficacious in wound-healing and are protective of normal tissues.

**Conclusions:** Our results reveal that $Tb_4O_7$ NPs have intrinsic oxidase-like activity and show effective antibacterial ability both in vitro and in vivo. These findings demonstrate that $Tb_4O_7$ NPs are effective antibacterial agents and may have a potential application in wound healing.

**Keywords:** $Tb_4O_7$ nanoparticles, Oxidase, Reactive oxygen species, Antibacterial, Wound healing

## Background

Wound infection is an important cause of poor wound healing and its treatment often requires the use of antibiotics [1, 2]. However, excessive use of antibiotics may lead to the development of antibiotic-resistant bacteria, and may also cause side effects on human health, such as gastrointestinal disturbances. In recent years, developments in nanomaterial technology have provided an opportunity to develop novel antimicrobial agents. Due to the diversity in mechanisms of action against bacteria, bacterial cells are less likely to develop antibacterial resistance compared to existing antibiotics [3–5]. However, most of these nanomaterials have application limitations, such as cytotoxicity, not biocompatible for human use, and environmental concerns.

Nanozymes are nanomaterials that catalyze the same reactions originally catalyzed by natural enzymes in biological systems [6–8]. Over the past several years, a wide variety of nanomaterials, such as noble metals [9–11], metal oxides [12–14], and carbon nanomaterials [15–18], have been explored as potential nanozymes. Based on their intrinsic enzyme-like activity, several nanozymes have been used in antibacterial applications [19–23]. For instance, platinum nanomaterials have shown effective antibacterial activity in the presence of hydrogen

*Correspondence: fsh729@sxu.edu.cn; panyue@mail.sysu.edu.cn; xtian@suda.edu.cn
†Chen Li, Yurong Sun and Xiaoping Li contributed equally to this work
[1] School for Life Science, Shanxi University, Taiyuan 030006, China
[2] Guangdong Provincial Key Laboratory of Malignant Tumor Epigenetics and Gene Regulation, Department of Radiation Oncology, Medical Research Center, Sun Yat-Sen Memorial Hospital, Sun Yat-Sen University, Guangzhou 510120, China
[5] State Key Laboratory of Radiation Medicine and Protection, School for Radiological and Interdisciplinary Sciences (RAD-X), Collaborative Innovation Center of Radiation Medicine of Jiangsu Higher Education Institutions, Soochow University, Suzhou 215123, China
Full list of author information is available at the end of the article

peroxide ($H_2O_2$) [24]. The antibacterial activity of these nanozymes are attributed primarily to their oxidase- and peroxidase-like activities that catalyze the production of hydroxyl radicals (·OH) in the presence of exogenous $H_2O_2$ and enhance the cellular levels of reactive oxygen species (ROS) within bacteria cells. Fang et al. also showed that palladium nanomaterials with oxidase- and peroxidase-like activities displayed effective antibacterial activity in the presence of $H_2O_2$ [25]. Although many reported enzyme-like nanomaterials have been proposed as novel antibacterial agents, the high price and persistence in living tissues are still important issues. Moreover, the application of $H_2O_2$ in human wound disinfection is harmful to healthy tissue and may delay wound healing [26].

Terbium oxide nanoparticles ($Tb_4O_7$ NPs) have been extensively used as precursors for the synthesis of lanthanide nanophosphors and superconductor materials [27, 28]. For example, $Tb_4O_7$ complexed with reduced graphene oxide composite exhibit typical green emission of terbium ions as well as the blue self-luminescence of graphene [28]. In addition, it has been found that $Tb_4O_7$ NPs can be used as analytical reagents for food analysis [29]. Compared with noble metal nanomaterials, $Tb_4O_7$ NPs are easier to synthesize and are less expensive. However, a review of scientific literature was unable to find any studies that described the enzyme-like activity of $Tb_4O_7$ NPs and their applications as antibacterial agents. In this paper, we show that $Tb_4O_7$ NPs have an intrinsic oxidase-like activity at acidic pH values, as they quickly oxidize a series of organic substrates in the absence of $H_2O_2$. We then demonstrate the relationship between the oxidase-like property of $Tb_4O_7$ NPs and their antibacterial activity with in vitro studies. Finally, the effects of $Tb_4O_7$ NPs on wound disinfection and healing are evaluated in in vivo studies using a wound infection mouse model.

## Materials and methods

### Chemicals and materials

$Tb_4O_7$ NPs were purchased from US Research Nanomaterials, Inc. (TX, USA). 3,3,5,5-tetramethylbenzidinedihydrochloride (TMB), diammonium 2,2′-azino-bis(3-ethylbenzothiazoline-6-sulfonate) (ABTS), *o*-phenylenediamine (OPD), and Lipid Peroxidation MDA Assay Kit were all purchased from Sigma-Aldrich (St. Louis, MO). The Live/Dead BacLight bacterial viability kit and 2′,7′-dichlorodihydrofluorescein diacetate (DCFH-DA) were obtained from Thermo Fisher Scientific, Inc. (MA, USA). 5-tert-butoxycarbonyl-5-methyl-1-pyrroline-*N*-oxide (BMPO) and Cell Counting Kit-8 (CCK-8) were obtained from Dojindo Laboratories (Kumamoto, Japan). *Escherichia coli* (*E. coli*) and *Staphylococcus aureus* subsp. *aureus* (*S. aureus*) were obtained from the China General Microbiological Culture Collection Center (CGMCC, Beijing, China). Human umbilical vein endothelial cells (HUVECs) were purchased from the American Type Culture Collection (ATCC, MD, USA).

### Characterization of $Tb_4O_7$ NPs

The hydrodynamic size and zeta potential of the $Tb_4O_7$ NPs were measured using a Zetasizer Nano-ZS (Malvern, UK). The morphology and size of the $Tb_4O_7$ NPs were characterized using a transmission electron microscopy (TEM, Tecnai G-20, FEI). The UV–vis absorption spectrum was recorded on a spectrophotometer (UV-3600, Shimadzu).

### Electron spin resonance spectroscopic measurements

The electron spin resonance (ESR) measurements were carried out using a Bruker EMX ESR spectrometer according to our previous study [3, 9]. The final concentration of each component is described in each figure caption. All the ESR measurements were carried out at ambient temperature.

### Measurement of intracellular ROS

After $Tb_4O_7$ NPs (100 μg/mL) treatment, bacteria ($1 \times 10^9$ CFU/mL) were collected by centrifugation and incubated with DCFH-DA (10 μM) for 30 min at dark, and stained bacteria were visualized with a confocal laser microscopy.

### Cytotoxicity experiments

HUVECs were employed for investigating the cytotoxicity of $Tb_4O_7$ NPs. HUVECs were seeded at a density of $1 \times 10^5$ cells/well in 96-well plates and incubated overnight. The HUVECs were then incubated with $Tb_4O_7$ NPs (0–100 μg/mL) for 24 h, and cell viability was measured by MTT assay.

### Mice injury model

BALB/c mice (8 weeks) were purchased from Pengsheng. On the day 0, the mice were anesthetized using 10% chloral hydrate. Then, the dorsal hair of mouse was shaved, full-thickness skin wounds with the diameter of 10 mm were created on the back of each mouse. After 24 h (day 1), the mice were treated with 50 μL PBS or $Tb_4O_7$ NPs (100 μg/mL). The $Tb_4O_7$ NPs were dripping on the surface of the wound.

### Hemolysis test

Fresh blood was collected under sterile conditions from healthy BALB/c mice (n = 5) into an anticoagulation tube. The red blood cells were precipitated by centrifugation at 2000 rpm for 10 min and washed three times with PBS

buffer solution to obtain red blood cells. The appropriate amount of red blood cells was diluted five times with PBS buffer solution to prepare a red blood cell solution. 20 μL of the diluted red blood cell suspension was mixed with a series of different concentrations of $Tb_4O_7$ NPs (0–200 μg/mL); ultrapure water was used as control. All the above samples were incubated at 37 °C for 2 h, centrifuged at 2000 rpm for 10 min, imaged, and the supernatant after centrifugation was taken in a 96-well plate to measure the absorbance at 540 nm using a microplate reader. The hemolysis rate was calculated as follows:

$$\text{Hemolysis rate (\%)} = (\text{sample absorption} - \text{negative control absorption})/(\text{positive control absorption} - \text{negative control absorption}) \times 100\%, \text{ and hemolysis rate exceeding 5\% is considered hemolysis.}$$

## Results and discussion

### Characterization of $Tb_4O_7$ NPs

The $Tb_4O_7$ NPs used in the present study were purchased from US Research Nanomaterials, Inc. The physical characterization of $Tb_4O_7$ NPs is shown in Additional file 1: Figure S1 and included images of particle core size and shape captured by TEM, the mean and homogeneity of particle hydrodynamic size by dynamic light scattering (DLS), and particle absorption spectrum by UV–vis. According to TEM and DLS data, the dispersity of $Tb_4O_7$ NPs is poor. The mean core particle size of $Tb_4O_7$ NPs is approximately 200 nm (Additional file 1: Figure S1a, b); while the DLS result of $Tb_4O_7$ NPs is around 400 nm (Additional file 1: Figure S1c). This is mainly due to the size measured by DLS was a hydrodynamic size, and therefore the nanoparticles showed a larger hydrodynamic volume due to solvent effect in the hydrated state. The zeta potential value of $Tb_4O_7$ NPs is 31.6 mV in water. The UV–vis spectrum of $Tb_4O_7$ NPs is shown in Additional file 1: Figure S1d.

### Catalytic activity of $Tb_4O_7$ NPs as oxidase mimetics

The oxidase-like activity of $Tb_4O_7$ NPs was evaluated using the substrate TMB. The UV–vis spectroscopy measurements show time-dependent increases in TMB oxidation catalyzed by $Tb_4O_7$ NPs, yielding a blue-colored product (Fig. 1a, b). In addition, $Tb_4O_7$ NPs can also catalyze the oxidation of ABTS and OPD (Fig. 1a).

We used the oxidation of TMB as a model reaction and found that the catalytic efficiency of the $Tb_4O_7$ NPs is dependent on TMB concentrations, pH and temperature (Fig. 1c and Additional file 1: Figure S2). As shown

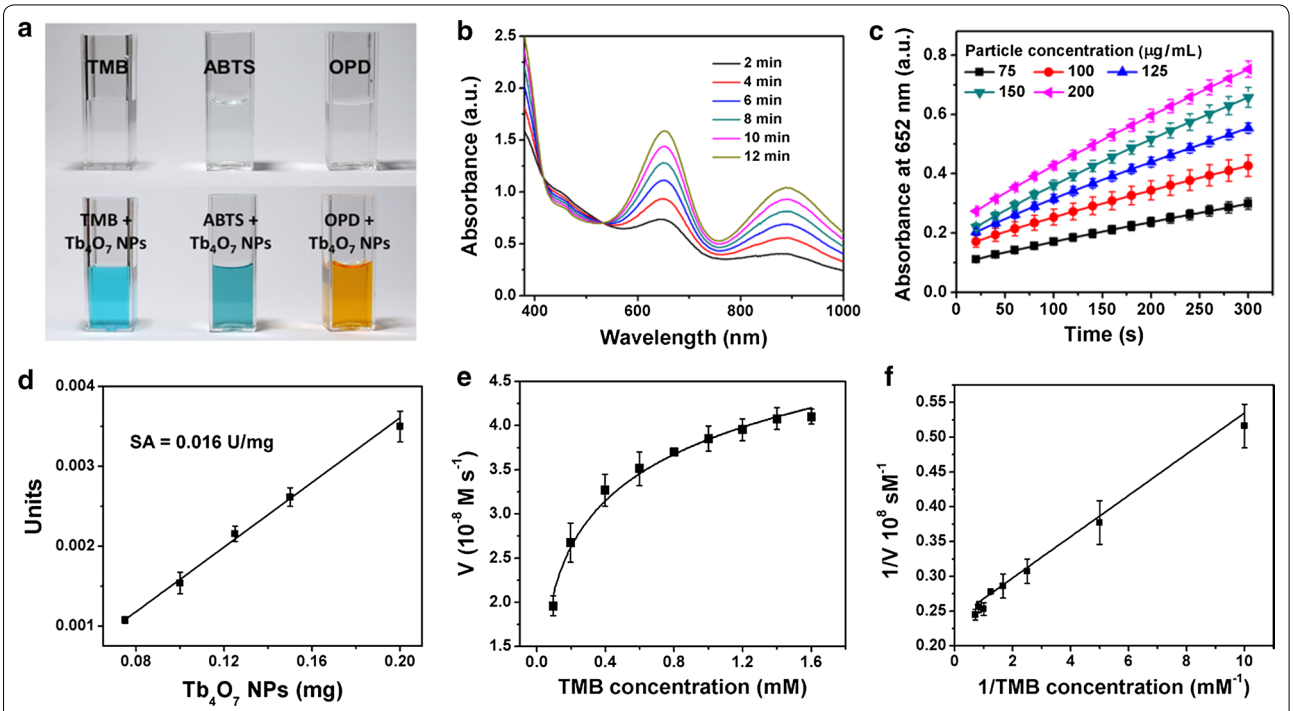


**Fig. 1** Oxidase-like activity of $Tb_4O_7$ NPs. **a** A photograph showing the capability of the $Tb_4O_7$ NPs in catalyzing the oxidations of TMB, ABTS, and OPD that produce colored products. **b** Time-dependent absorption spectra of TMB catalyzed by $Tb_4O_7$ NPs. **c** Absorbance at 652 nm measured from samples containing TMB and different concentrations of $Tb_4O_7$ NPs. **d** The specific activities of $Tb_4O_7$ NPs. Steady-state kinetic assays of $Tb_4O_7$ NPs (**e**, **f**). **e** TMB concentration dependence of initial reaction velocity. **f** Double-reciprocal plot generated from (**d**)

in Additional file 1: Figure S2a, $Tb_4O_7$ NPs exhibit excellent catalytic activity over a broad temperature range (25–60 °C). Moreover, an acidic condition (pH = 3.6) is conducive to the oxidase-like activity of $Tb_4O_7$ NPs (Additional file 1: Figure S2b). We adopted pH 3.6 and 25 °C (room temperature) as the standard conditions for subsequent studies.

Next, we determined the apparent steady-state kinetic parameters for the reaction of $Tb_4O_7$ NPs with TMB. Typical Michaelis–Menten curves were established (Fig. 1d). The curves were then fitted to the double-reciprocal Lineweaver–Burk plots (Fig. 1e), from which the kinetic parameters shown in Table 1 were determined.

### Effects of $Tb_4O_7$ NPs on the anti-oxidant defense system

The above results show that $Tb_4O_7$ NPs have oxidase-like activity oxidizing TMB, ABTS, and OPD in the absence of $H_2O_2$. We predict that $Tb_4O_7$ NPs would deplete intracellular antioxidants and, eventually, disrupt the antioxidant defense systems of bacteria. To test this hypothesis, we examined the effects of $Tb_4O_7$ NPs on ascorbic acid (AA) oxidation in vitro. AA is an important endogenous bacterial antioxidant that prevents cellular damage from ROS. AA can be oxidized to form an intermediate ascorbyl radical (·AA), which is detectable by ESR spectroscopy [9]. As shown in Fig. 2a, the oxidation of AA was negligible within 10 min, while in the presence of $Tb_4O_7$ NPs the system showed a time-dependent increase in the ESR signal intensity in the first 8 min and then decreased over time. These results indicate that $Tb_4O_7$ NPs can accelerate AA oxidation.

**Table 1 The kinetic constants of $Tb_4O_7$ NPs**

| | [E] (M) | $K_m$ (M) | $V_{max}$ (M/s) | $K_{cat}$ ($s^{-1}$) | $K_{cat}/K_m$ ($M^{-1}$ $S^{-1}$) |
|---|---|---|---|---|---|
| $Tb_4O_7$ NPs | $7.04 \times 10^{-10}$ | $1.24 \times 10^{-4}$ | $4.31 \times 10^{-8}$ | $1.61 \times 10^{-4}$ | 1.30 |

[E] is the concentration of $Tb_4O_7$ NPs. The particle number of $Tb_4O_7$ NPs is calculated using the density and diameter of $Tb_4O_7$ NPs. Dividing the particle number by the Avogadro constant is the molar concentration of $Tb_4O_7$ NPs

In the substrate oxidation mechanism of most oxidases in nature, oxygen acts as the electron acceptor and is reduced to $H_2O_2$. To gain a better understanding of the oxidation of AA by $Tb_4O_7$ NPs, we examined whether the catalytic oxidation product of $Tb_4O_7$ NPs and AA produced $H_2O_2$. As shown in Additional file 1: Figure S3, a marked increase of $H_2O_2$ was detected in the presence of $Tb_4O_7$ compared to control (AA alone). Moreover, the production of $H_2O_2$ was $Tb_4O_7$ concentration-dependent.

Previous studies have demonstrated that several kinds of nanoparticles are capable of catalyzing the production of hydroxyl radicals by $H_2O_2$ [30, 31]. Therefore, we determined whether $Tb_4O_7$ NPs would catalyze the production of hydroxyl radicals by $H_2O_2$ using ESR spectroscopy. We selected BMPO as the capture agent, since BMPO can capture hydroxyl radicals to form BMPO/·OH adducts indicated by the presence of four characteristic lines on the ESR spectrum. As shown in Fig. 2b, the characteristic ESR signals of BMPO/·OH were negligible in the absence of $Tb_4O_7$ NPs. However, the addition of $Tb_4O_7$ NPs resulted in a strong ESR spectrum that displayed the four characteristic lines (1:2:2:1) of BMPO/·OH. These results clearly show that $Tb_4O_7$ NPs can be used as a catalyst in the decomposition of $H_2O_2$ to produce hydroxyl radicals.

Taken together, our results confirm that $Tb_4O_7$ NPs are capable of catalyzing the oxidation of biologically

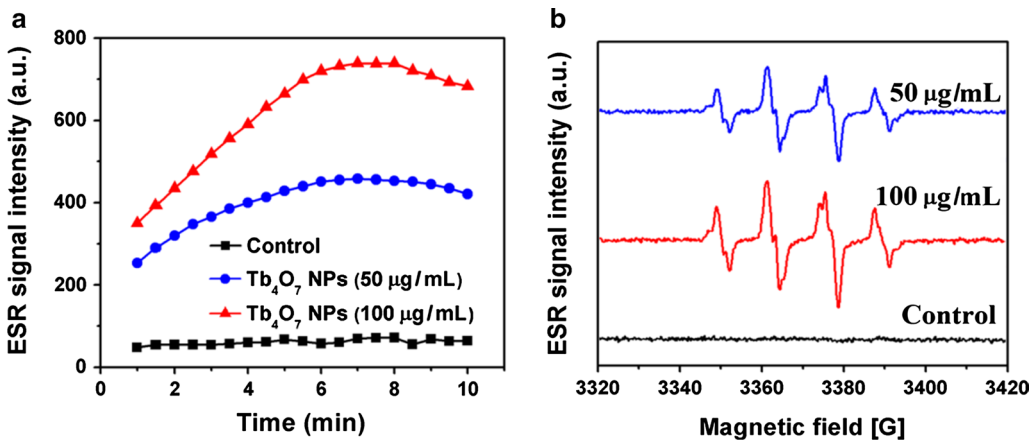


**Fig. 2** **a** Oxidation of AA by $Tb_4O_7$ NPs. **b** ESR spectra of BMPO/·OH generated from a sample solution containing 25 mM BMPO, 1 mM $H_2O_2$ in the absence (control) and presence of different concentrations of $Tb_4O_7$ NPs

relevant antioxidant agents, resulting in the production of $H_2O_2$. Moreover, $Tb_4O_7$ NPs can further catalyze the production of hydroxyl radicals via the decomposition of $H_2O_2$.

#### Antibacterial activity of $Tb_4O_7$ NPs

Both $H_2O_2$ and hydroxyl radicals have strong oxidizing ability and can oxidize biological macromolecules, such as proteins and phospholipids [32]. Our study found that $Tb_4O_7$ NPs with oxidase-like activity can catalyze the production of $H_2O_2$ and further produce hydroxyl radicals. Therefore, the oxidase-like activity of the $Tb_4O_7$ NPs makes them potentially useful as antibacterial agents. We evaluated the antibacterial activity of $Tb_4O_7$ NPs against *E. coli* and *S. aureus*. A colony-forming units plate counting method was used to determine the antibacterial ability (Fig. 3a, b). As compared to the PBS control group, $Tb_4O_7$ NPs exhibited potent antimicrobial activity against both *S. aureus* and *E. coli* in a concentration-dependent manner. At a concentration of 25 μg/mL, $Tb_4O_7$ NPs exhibited only modest antibacterial effects against *S. aureus*; more than 80% of the bacterial cells survived. However, when the concentration of $Tb_4O_7$ NPs was increased to 100 μg/mL, nearly 90% of the *S. aureus* were killed. A similar trend of antibacterial effects were observed towards the *E. coli*.

To further investigate the interaction between $Tb_4O_7$ NPs and bacteria, a fluorescent-based cell live/dead assay was conducted. As shown in Fig. 3c, d, $Tb_4O_7$ NPs exhibited significant antibacterial activity against both *S. aureus* and *E. coli*, which was consistent with the aforementioned results. The exposure of *S. aureus* cells to $Tb_4O_7$ NPs at a concentration of 100 μg/mL resulted in nearly 100% lethality, as evidenced by the dominant red fluorescent signal. At a concentration of 50 μg/mL, $Tb_4O_7$ NPs completely inhibited the bacterial growth of *E. coli*.

The morphology and membrane integrity of bacteria were then determined by SEM (Fig. 3c, d). Untreated *S. aureus* displayed a typical rod-shaped structure with a continuous, smooth surface. When exposure to the 50 μg/mL of $Tb_4O_7$ NPs, the *S. aureus* bacterial cell walls became partially wrinkled and discontinuance. Notably, after treatment with 100 μg/mL of $Tb_4O_7$ NPs, the *S. aureus* bacterial cell walls showed much more pronounced damage, indicating stronger antibacterial effects at higher concentrations of $Tb_4O_7$ NPs. A similar tendency was found for *E. coli*. The loss of membrane integrity of *E. coli* was observed at concentrations lower than 100 μg/mL of $Tb_4O_7$ NPs treatment. Moreover, $Tb_4O_7$ NPs were observed by SEM and SEM-energy dispersive X-ray spectroscopy (EDS) to aggregate on the surfaces of *S. aureus* and *E. coli* (Additional file 1: Figure S4).

It is known that the proton motive force decreases the local pH (as low as pH 3.0) in the cytoplasm and membrane of bacteria cells [33, 34]. Since we found that $Tb_4O_7$ NPs exhibit oxidase-like activity under acidic conditions, we speculate that the antibacterial mechanism of $Tb_4O_7$ NPs may arise from their oxidase activity to accelerate the process of bacterial cell oxidation and consumption of antioxidant biomolecules, leading to a reduction of oxygen products including $H_2O_2$ along with other antibacterial activity from the accumulation of ROS. To confirm this hypothesis, the intracellular levels of ROS were determined using the florescent probe, DCFH-DA (Fig. 4). For both *S. aureus* and *E. coli*, the untreated cells showed extremely weak fluorescence, indicating low levels in the formation of intracellular ROS. In contrast, bacterial cells exposed to $Tb_4O_7$ NPs showed high levels of ROS formed within the cellular cytoplasm, as evidenced by the strong fluorescence signal. We also found that the generation of ROS is $Tb_4O_7$ NPs dose-dependent (Additional file 1: Figure S5).

#### In vivo wound disinfection effect of $Tb_4O_7$ NPs

The above findings suggest that $Tb_4O_7$ NPs may have role as an antibacterial agent for bacterial infections in vivo. To assess the antibacterial capacity of $Tb_4O_7$ NPs in vivo, a wound infection model was constructed using BALB/c mice. A wound was introduced on the back of the mouse and an infection was established by implanting *S. aureus* into the wounded area. After infection was established, PBS or $Tb_4O_7$ NPs were applied to the infected wound. Figure 5a, b shows the progress of the wounds. Compared with the control (PBS treatment) group after 3 days, the wound area was reduced under $Tb_4O_7$ NPs treatment. After treating of 7 days with $Tb_4O_7$ NPs treatment, the wounds were nearly healed completely. In contrast, obvious scab was observed from the control group, indicating incomplete recovery.

#### Biosafety of $Tb_4O_7$ NPs

Biosafety is an important factor for antimicrobial agents designers. To assess the biosafety of $Tb_4O_7$ NPs, we first determined the effects of $Tb_4O_7$ NPs on red blood cells and HUVECs in vitro. The effect of $Tb_4O_7$ NPs on cell membrane disrupt was first determined by a red blood cell hemolysis assay. As shown in Fig. 6a, pure water can cause severe red blood cells hemolysis within 2 h. In contrast, the introduction of $Tb_4O_7$ NPs did not cause signs of hemolysis. In this experimental result, the hemolysis rate was still less than 1% at a concentration of 100 μg/mL, which fully demonstrated that $Tb_4O_7$ NPs have good blood compatibility. Meanwhile, the cytotoxicity tests on

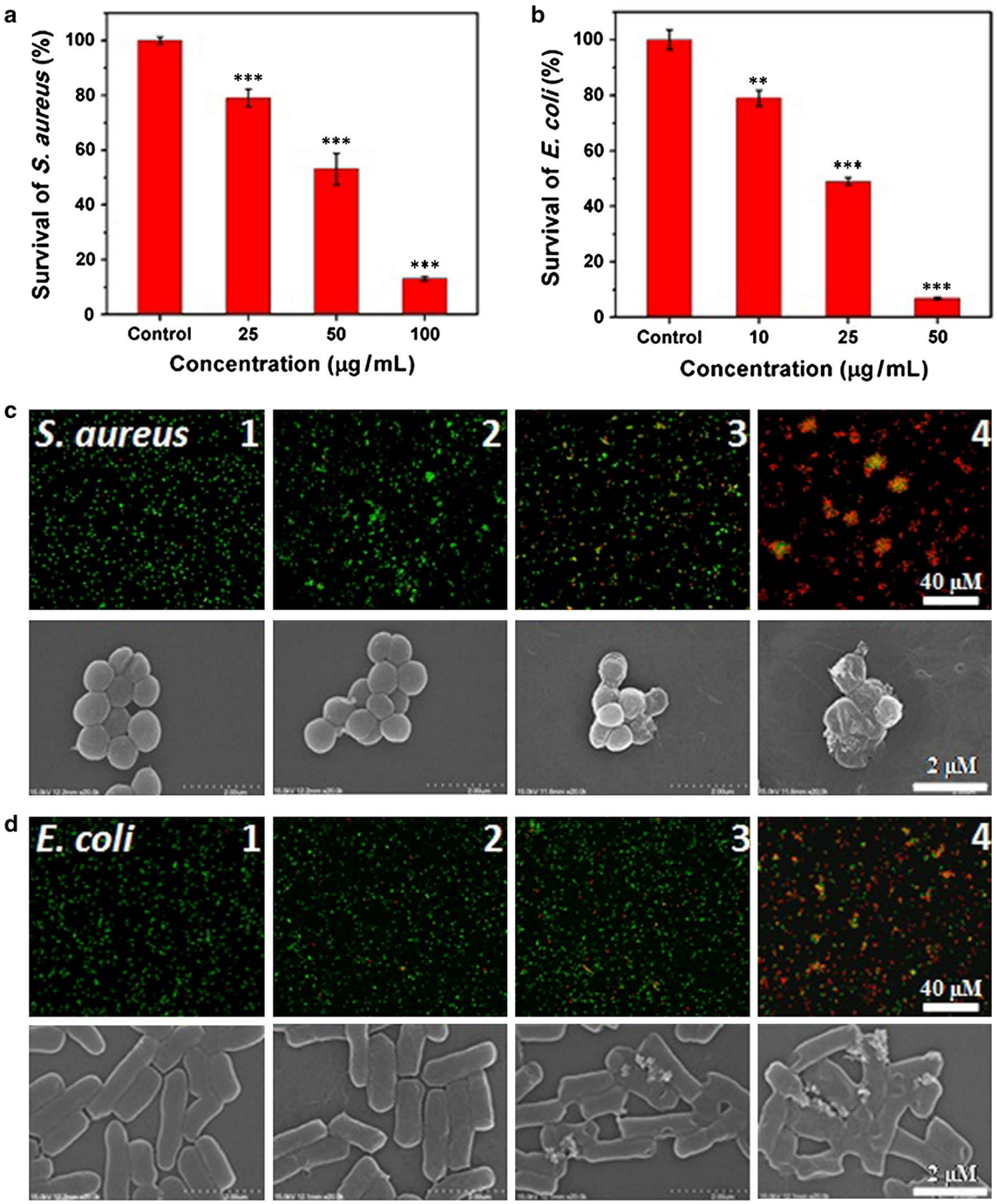


**Fig. 3** The effect of $Tb_4O_7$ NPs on survival rates of bacteria **a** CFUs of *S. aureus* following incubation with $Tb_4O_7$ NPs; **b** CFUs of *E. coli* following incubation with $Tb_4O_7$ NPs; **c** Representative fluorescence and SEM images of *S. aureus* after $Tb_4O_7$ NPs treatments. Bacterial cells were treated with 1) PBS as control, 2) 25 μg/mL $Tb_4O_7$ NPs, 3) 50 μg/mL $Tb_4O_7$ NPs or 4) 100 μg/mL $Tb_4O_7$ NPs; **d** Representative fluorescence and SEM images of *E. coli* after $Tb_4O_7$ NPs treatments. Bacterial cells were treated with 1) PBS as control, 2) 10 μg/mL $Tb_4O_7$ NPs, 3) 25 μg/mL $Tb_4O_7$ NPs or 4) 50 μg/mL $Tb_4O_7$ NPs. $^{**}p < 0.01$ and $^{***}p < 0.001$ vs control

mammalian cells HUVECs further confirm the biosafety of $Tb_4O_7$ NPs (Fig. 6b).

Then, the biosafety of $Tb_4O_7$ NPs in vivo were determined. As shown in Fig. 7a, the indicators in blood were within the normal range. The major mouse organs (heart, liver, spleen, lung, and kidney) were formalin-fixed and processed for the evaluation of H&E sections by

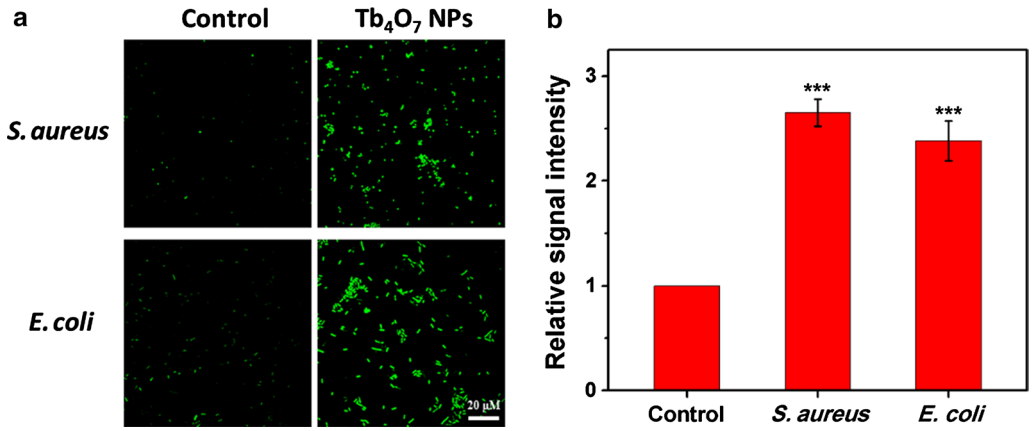


**Fig. 4** **a** Fluorescence images of bacterial cells. **b** Analysis of the ROS levels by microplate reader. ***$p < 0.001$ vs control

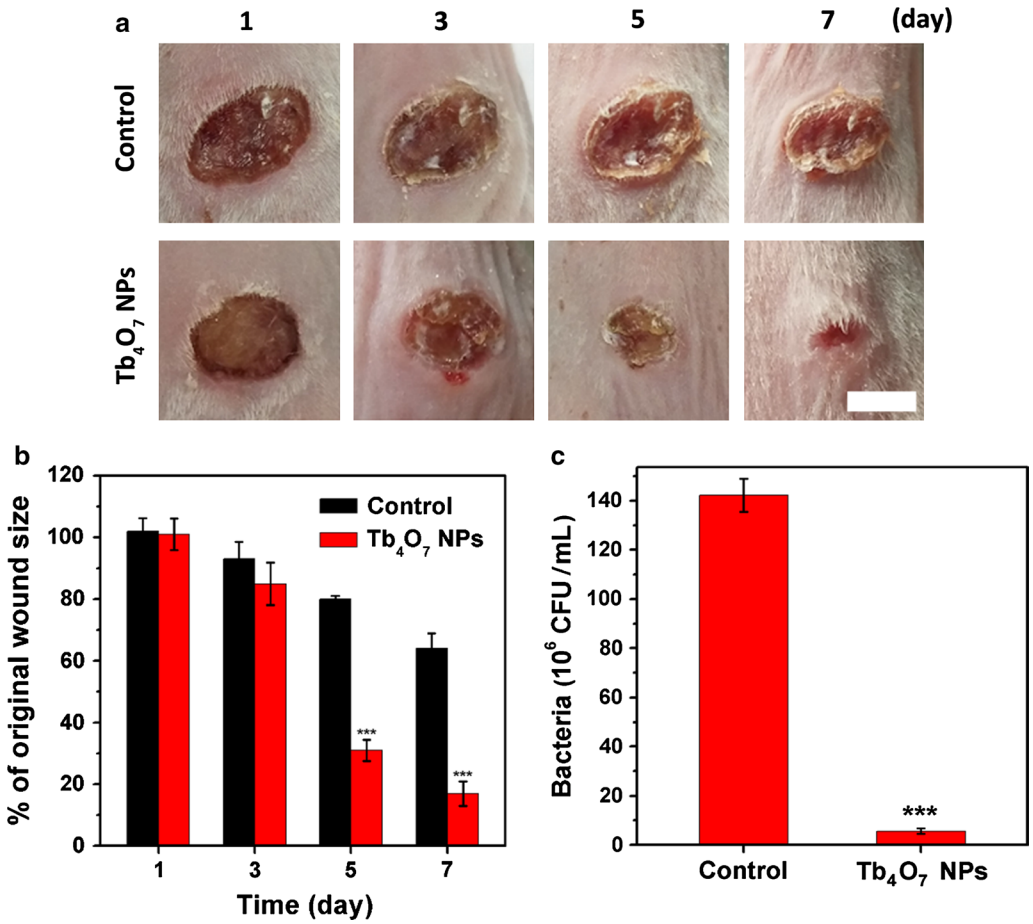


**Fig. 5** **a** Photographs of wounds on the backs of mice in control (PBS) and $Tb_4O_7$ NPs treatment groups (n = 5). Scale bar: 5 mm. **b** Related wound size in each treatment group. **c** Bacterial number of infected wounds on the 7th day. ***$p < 0.001$ vs control

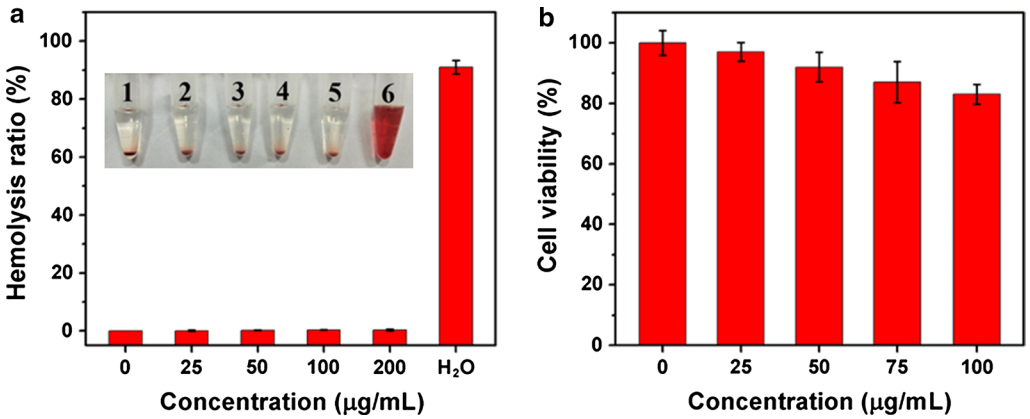


**Fig. 6** **a** The hemolysis ratio of red blood cells. The insert images of tubes containing red blood cells solution show the direct observation of hemolysis. Tube 1: PBS buffer; Tube 2–5: 25, 50, 100, and 200 μg/mL $Tb_4O_7$ NPs; Tube 6: ultrapure water. **b** MTT assays determined cell viability of HUVECs after $Tb_4O_7$ NPs treatment

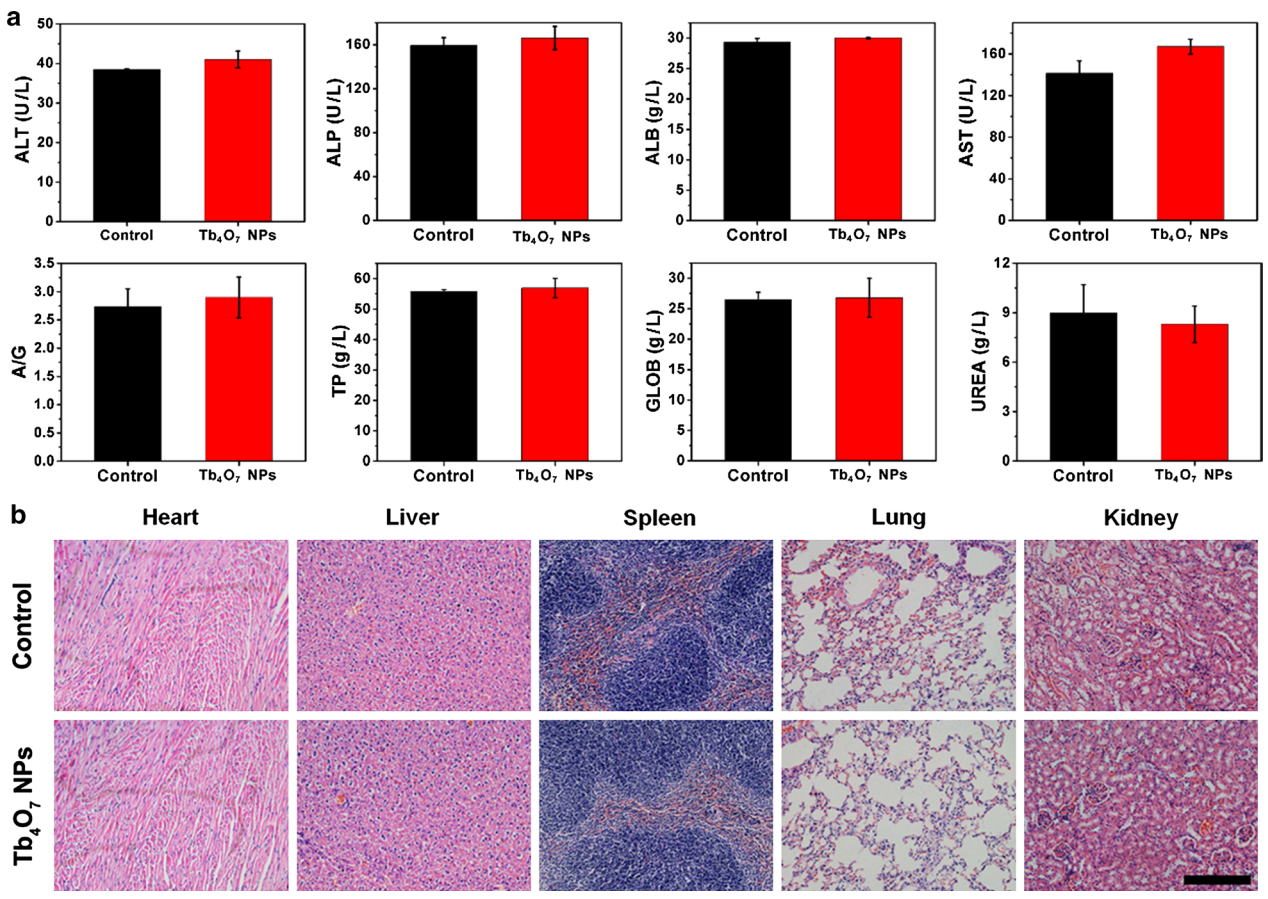


**Fig. 7** In vivo toxicity of $Tb_4O_7$ NPs. **a** The blood biochemistry data of the mice treated with $Tb_4O_7$ NPs after 7 d (n = 5). **b** Histological data (H&E staining images) are obtained from the major organs of mice treated with $Tb_4O_7$ NPs after 7 d. Scale bar = 100 μm

histopathology (Fig. 7b). No obvious mouse organ damage was observed from $Tb_4O_7$ NPs treatment.

## Conclusions

In summary, this study demonstrates for the first time that $Tb_4O_7$ NPs exhibit oxidase-like activity. In addition, the results of this study established a relationship between the oxidase-like enzyme activity of $Tb_4O_7$ NPs and their antibacterial properties. The data collected from this work revealed that the oxidase-like activity of $Tb_4O_7$ NPs was able to function with a variety of substrates, including biomolecules, and resulted in the generation of ROS, which further enhanced their antibacterial activity. The application of the antibacterial activities of $Tb_4O_7$ NPs were demonstrated in a wound infection mouse model. Our study provides evidence that $Tb_4O_7$ NPs can be utilized as an efficient antibacterial agent and the potential applications in wound healing are promising.

## Additional file

**Additional file 1: Figure S1.** Characterization of $Tb_4O_7$ NPs. **Figure S2.** The oxidase-like catalytic activity of the $Tb_4O_7$ NPs. **Figure S3.** The concentration of $H_2O_2$ generated in the catalytic system. **Figure S4.** SEM-EDS elemental images. **Figure S5.** ROS levels of *S. aureus*.

### Abbreviations

$Tb_4O_7$: terbium oxide; NPs: nanoparticles; $H_2O_2$: hydrogen peroxide; ROS: reactive oxygen species; ABTS: diammonium 2,2′-azino-bis(3-ethylbenzothiazoline-6-sulfonate); OPD: *o*-phenylenediamine; AA: ascorbic acid; DCFH-DA: 2′,7′-dichlorodihydrofluorescein diacetate; BMPO: 5-tert-butoxycarbonyl-5-methyl-1-pyrroline-*N*-oxide; CCK-8: Cell Counting Kit-8; *E. coli*: *Escherichia coli*; *S. aureus*: *Staphylococcus aureus* subsp. *aureus*; HUVEC: human umbilical vein endothelial cells; TEM: transmission electron microscopy; ESR: electron spin resonance; CFUs: colony forming units; PI: propidium iodide; SEM: scanning electron microscope; DLS: dynamic light scattering; EDS: energy dispersive X-ray spectroscopy.

### Authors' contributions

CL, YS, and XL prepared and performed the experiments. YS, XL and YL analyzed the data and interpreted the results. XT, SF and YP conceived and supervised the study. The manuscript was written by XT and XJ, and revised critically by JY and MB. All authors read and approved the final manuscript.

### Author details

[1] School for Life Science, Shanxi University, Taiyuan 030006, China. [2] Guangdong Provincial Key Laboratory of Malignant Tumor Epigenetics and Gene Regulation, Department of Radiation Oncology, Medical Research Center, Sun Yat-Sen Memorial Hospital, Sun Yat-Sen University, Guangzhou 510120, China. [3] Division of Analytical Chemistry, Office of Regulatory Science, Center for Food Safety and Applied Nutrition, U.S. Food and Drug Administration, College Park, MD 20740, USA. [4] Division of Biochemical Toxicology, National Center for Toxicological Research, U.S. Food and Drug Administration, Jefferson, AR 72079, USA. [5] State Key Laboratory of Radiation Medicine and Protection, School for Radiological and Interdisciplinary Sciences (RAD-X), Collaborative Innovation Center of Radiation Medicine of Jiangsu Higher Education Institutions, Soochow University, Suzhou 215123, China.

### Acknowledgements

Not applicable.

### Competing interests

The authors declare that they have no competing interests.

### Availability of data and materials

All data generated or analyzed during this study are included in this published article and its additional file.

### Consent for publication

All authors agree to be published.

### Ethics approval and consent to participate

The protocols and the use of animals were approved by and in accordance with the animal welfare committee of Soochow University.

### Funding

This work is partially supported by the National Natural Science Foundation of China (31400862), a project funded by the Priority Academic Program Development of Jiangsu Higher Education Institutions (PAPD), Jiangsu Provincial Key Laboratory of Radiation Medicine and Protection, Guangdong Science and Technology Department (2017B030314026). This article is not an official U.S. FDA guidance or policy statement. No official support or endorsement by the U.S. FDA is intended or should be inferred.

## Publisher's Note



Received: 25 January 2019 Accepted: 8 April 2019
Published online: 16 April 2019

### References

1. Fischbach MA, Walsh CT. Antibiotics for emerging pathogens. Science. 2009;325:1089–93.
2. Kohanski MA, Dwyer DJ, Collins JJ. How antibiotics kill bacteria: from targets to networks. Nat Rev Microbiol. 2010;8:423–35.
3. Tian X, Jiang X, Welch C, Croley TR, Wong TY, Chen C, Fan S, Chong Y, Li R, Ge C, Chen C, Yin JJ. Bactericidal effects of silver nanoparticles on lactobacilli and the underlying mechanism. ACS Appl Mater Interfaces. 2018;10:8443–50.
4. Mahmoudi M, Serpooshan V. Silver-coated engineered magnetic nanoparticles are promising for the success in the fight against antibacterial resistance threat. ACS Nano. 2012;6:2656–64.
5. Panacek A, Kvitek L, Smekalova M, Vecerova R, Kolar M, Roderova M, Dycka F, Sebela M, Prucek R, Tomanec O, Zboril R. Bacterial resistance to silver nanoparticles and how to overcome it. Nat Nanotechnol. 2018;13:65–71.
6. Jiang B, Duan D, Gao L, Zhou M, Fan K, Tang Y, Xi J, Bi Y, Tong Z, Gao GF, Xie N, Tang A, Nie G, Liang M, Yan X. Standardized assays for determining the catalytic activity and kinetics of peroxidase-like nanozymes. Nat Protoc. 2018;13:1506–20.
7. Gao L, Fan K, Yan X. Iron oxide nanozyme: a multifunctional enzyme mimetic for biomedical applications. Theranostics. 2017;7:3207–27.
8. Wang X, Hu Y, Wei H. Nanozymes in bionanotechnology: from sensing to therapeutics and beyond. Inorg Chem Front. 2016;3:41–60.
9. Chen C, Fan SH, Li C, Chong Y, Tian X, Zheng JW, Fu PP, Jiang XM, Wamer WG, Yin JJ. Platinum nanoparticles inhibit antioxidant effects of vitamin C via ascorbate oxidase-mimetic activity. J Mater Chem B. 2016;4:7895–901.
10. Luo W, Zhu C, Su S, Li D, He Y, Huang Q, Fan C. Self-catalyzed self-limiting growth of glucose oxidase-mimicking gold nanoparticles. ACS Nano. 2010;4:7451–8.
11. Xia X, Zhang J, Lu N, Kim M, Ghal K, Xu W, McKenzie E, Liu J, Ye H. Pd-Ir core-shell nanocubes: a type of highly efficient and versatile peroxidase mimic. ACS Nano. 2015;9:9994–10004.
12. Yao J, Cheng Y, Zhou M, Zhao S, Lin S, Wang X, Wu J, Li S, Wei H. ROS scavenging $Mn_3O_4$ nanozymes for in vivo anti-inflammation. Chem Sci. 2018;9:2927–33.

13. Ghosh S, Roy P, Karmodak N, Jemmis ED, Mugesh G. Nanoisozymes: crystal-facet-dependent enzyme-mimetic activity of $V_2O_5$ nanomaterials. Angew Chem Int Ed Engl. 2018;57:4510–5.
14. Singh N, Savanur MA, Srivastava S, D'Silva P, Mugesh GA. Redox modulatory $Mn_3O_4$ nanozyme with multi-enzyme activity provides efficient cytoprotection to human cells in a Parkinson's disease model. Angew Chem Int Ed Engl. 2017;56:14267–71.
15. Lin L, Song X, Chen Y, Rong M, Zhao T, Wang Y, Jiang Y, Chen X. Intrinsic peroxidase-like catalytic activity of nitrogen-doped graphene quantum dots and their application in the colorimetric detection of $H_2O_2$ and glucose. Anal Chim Acta. 2015;869:89–95.
16. Zheng AX, Cong ZX, Wang JR, Li J, Yang HH, Chen GN. Highly-efficient peroxidase-like catalytic activity of graphene dots for biosensing. Biosens Bioelectron. 2013;49:519–24.
17. Wang H, Liu C, Liu Z, Ren J, Qu X. Specific oxygenated groups enriched graphene quantum dots as highly efficient enzyme mimics. Small. 2018;14:e1703710.
18. Hassanzadeh J, Khataee A. Ultrasensitive chemiluminescent biosensor for the detection of cholesterol based on synergetic peroxidase-like activity of $MoS_2$ and graphene quantum dots. Talanta. 2018;178:992–1000.
19. Wang Z, Dong K, Liu Z, Zhang Y, Chen Z, Sun H, Ren J, Qu X. Activation of biologically relevant levels of reactive oxygen species by Au/g-$C_3N_4$ hybrid nanozyme for bacteria killing and wound disinfection. Biomaterials. 2017;113:145–57.
20. Cai S, Jia X, Han Q, Yan X, Yang R, Wang C. Porous Pt/Ag nanoparticles with excellent multifunctional enzyme mimic activities and antibacterial effects. Nano Res. 2017;10:2056–69.
21. Tao Y, Ju E, Ren J, Qu X. Bifunctionalized mesoporous silica-supported gold nanoparticles: intrinsic oxidase and peroxidase catalytic activities for antibacterial applications. Adv Mater. 2015;27:1097–104.
22. Chen Z, Wang Z, Ren J, Qu X. Enzyme mimicry for combating bacteria and biofilms. Acc Chem Res. 2018;51:789–99.
23. Chen S, Quan Y, Yu YL, Wang JH. Graphene quantum dot/silver nanoparticle hybrids with oxidase activities for antibacterial application. ACS Biomater Sci Eng. 2017;3:313–21.
24. Ge C, Wu R, Chong Y, Fang G, Jiang X, Pan Y, Chen C, Yin JJ. Synthesis of Pt hollow nanodendrites with enhanced peroxidase-like activity against bacterial infections: implication for wound healing. Adv Funct Mater. 2018;28:1801484.
25. Fang G, Li W, Shen X, Perez-Aguilar JM, Chong Y, Gao X, Chai Z, Chen C, Ge C, Zhou R. Differential Pd-nanocrystal facets demonstrate distinct antibacterial activity against Gram-positive and Gram-negative bacteria. Nat Commun. 2018;9:129.
26. Loo AE, Wong YT, Ho R, Wasser M, Du T, Ng WT, Halliwell B. Effects of hydrogen peroxide on wound healing in mice in relation to oxidative damage. PLoS ONE. 2012;7:e49215.
27. Nahm CW. Varistor characteristics of $ZnO/V_2O_5/MnO_2/Nb_2O_5$ semiconducting ceramics with $Tb_4O_7$ addition. J Mater Sci Mater El. 2015;26:4144–51.
28. Gao H, Zhou Y, Chen KQ, Li XL. Synthesis of $Tb_4O_7$ complexed with reduced graphene oxide for Rhodamine-B absorption. Mater Res Bull. 2016;77:111–4.
29. Castillo-Garcia ML, Aguilar-Caballos MP, Gomez-Hens A. Application of Tb(4)O(7) nanoparticles for lasalocid and salicylate determination in food analysis. J Agric Food Chem. 2012;60:11741–7.
30. Tian X, Sun Y, Fan S, Boudreau M, Chen C, Ge C, Yin JJ. Photogenerated charge carriers in molybdenum disulfide quantum dots with enhanced antibacterial activity. ACS Appl Mater Interfaces. 2019;11:4858–66.
31. Tao W, Zhang H, Chong Y, Wamer WG, Yin JJ, Wu XC. Probing hydroxyl radical generation from $H_2O_2$ upon plasmon excitation of gold nanorods using electron spin resonance: molecular oxygen-mediated activation. Nano Res. 2016;9:1663–73.
32. Sun HJ, Gao N, Dong K, Ren JS, Qu XG. Graphene quantum dots-band-aids used for wound disinfection. ACS Nano. 2014;8:6202–10.
33. Koch AL. The pH in the neighborhood of membranes generating a protonmotive force. J Theor Biol. 1986;120:73–84.
34. Xiu ZM, Zhang QB, Puppala HL, Colvin VL, Alvarez PJ. Negligible particle-specific antibacterial activity of silver nanoparticles. Nano Lett. 2012;12:4271–5.